The competition between crystallization and phase separation in polymer blends: 2. Small-angle X-ray scattering studies on the crystalline morphology of poly(ε-caprolactone) in its blends with polystyrene

Y. Li* and B.-J. Jungnickel†
Deutsches Kunststoff-Institut, Darmstadt, Germany
(Received 10 December 1991; revised 10 March 1992)

The courses of crystallization and of demixing or mixing, respectively, can interfere and compete in polymer blends with a miscibility gap. Crystallization dominates at lower temperatures, possibly inhibiting rejection of the non-crystallizing component into the remaining melt and enhancing its concentration in the amorphous regions between the crystalline domains. Time-resolved small-angle X-ray scattering measurements on poly(ε-caprolactone)/polystyrene (PCL/PS) blends, this system exhibiting an upper critical solution temperature, reveal that the amorphous regions between the lamellae within the PCL spherulites nearly do not phase separate when passing the binodal composition. Instead, supersaturation of composition occurs. The initially bent lamellae flatten with time, and the supersaturated spherulite amophous phase post-crystallizes according to the insertion crystallization scheme on a timescale that is comparable to the overall crystallization rate.

(Keywords: polymer blends; poly(ε-caprolactone); polystyrene; phase separation; crystallization; kinetics; small-angle X-ray scattering; morphology; lamellar bundles; amorphous structure)

INTRODUCTION

In comparison to the pure components, polymer blends can exhibit a great variety of interesting and important new features when solidifying. These are due partly to the equilibrium thermodynamics of mixing, and partly to the blending-induced changes in crystallization kinetics. In particular, the kinetics of mixing or demixing, respectively, can interfere and compete with that of crystallization when the blend system has a miscibility gap. Which of these phase transitions dominates and, consequently, which supermolecular morphology and phase structure result, will then depend on the composition and on the thermal boundary conditions[1–5]. This issue is clearly observable and has been investigated already to some degree in the blend system poly(ε-caprolactone)/polystyrene (PCL/PS) where PCL is the only crystallizable component[1–3,6]. This blend exhibits an upper critical solution temperature (*UCST*), and the melting-point depression curve of the PCL intersects the miscibility gap[1] (*Figure 1*). The left branch of the binodal line lies at a composition that, essentially, consists of almost pure PS. The several supermolecular structures that result in this system under different preparation and thermal conditions have already been investigated by light microscopy[1–3].

One specific aspect is here of particular interest. Crystallization of PCL in an originally isotropic melt (which in turn can be one phase of a phase-separated structure; cf. *Figure 2a*) causes release of non-crystallizable PS that can either remain in the growing spherulites (*Figure 2b*) or be rejected by diffusion into the remaining melt, thus increasing its concentration in the melt (*Figure 2c*) until there the binodal composition is reached. In the first case it will depend on the degree of crystallinity within the spherulites, on the starting composition and on the relative rates of diffusion and spherulite growth, i.e. essentially on the actual crystallization temperature (*Figure 3*), whether a thermodynamically stable or a supersaturated homogeneous mixing is established in the amorphous regions of the spherulites, or whether there demixed PS droplets are created and inserted (*Figure 2d*). The development of additional crystalline lamellae by a process comparable to insertion crystallization (which is temporally delayed with respect to the main crystallization step because of the concentration dependence of crystallization rate) is also possible (*Figures 2e* and *14*). If PS can diffuse into the melt, a concentration gradient will arise around the growing spherulite, the width of which will again depend on the relative rates of crystallization and diffusion. This concentration distribution will in some cases reach the binodal composition at the spherulite surface, there causing demixing and, consequently, creation of droplets that consist of almost pure PS[1] (*Figure 2f*). These

*Present address: Molecular Simulations AG, Basel, Switzerland
†To whom correspondence should be addressed

0032-3861/93/010009-07
© 1993 Butterworth-Heinemann Ltd.

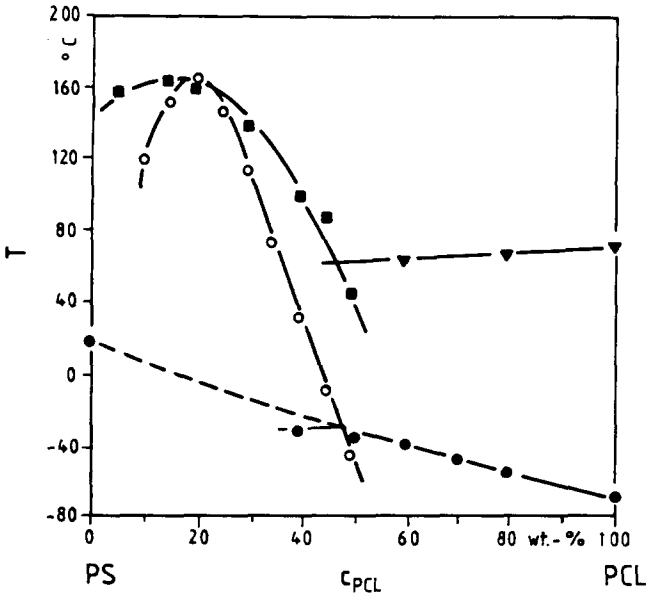

Figure 1 Phase diagram of the PCL/PS blend[1]. Sample materials according to *Table 1*. (■) Binodal; (○) spinodal; (▼) melt/crystal coexistence curve; (●) glass transition temperature; (– – –) glass transition temperatures of supersaturated blends calculated with the Fox equation[15]

processes and structures, clearly, are observable not only in the blend system PCL/PS but in all mixtures that exhibit a similar phase diagram.

Each of these solidification paths is linked with its own crystallization kinetics, which, in turn, influences the resulting crystalline and supermolecular morphology of the PCL. Whereas our earlier light microscopic investigations[1] monitored these features on a scale of micrometres, it is the aim of the present paper to report on these changes on a level that can be detected by small-angle X-ray scattering (SAXS) measurements. The first relates to the phase structure and the overall spherulitic structure, the latter to the internal structure of the spherulites. Of particular interest was the type of segregation or insertion into the spherulites of the PS released by crystallization. To this end, time-resolved SAXS investigations of the temporal development of the structure during isothermal crystallization using synchrotron radiation were performed. The results of non-isothermal crystallization experiments are described elsewhere[6].

Time-resolved SAXS measurements have been widely used in recent years in order to study the crystallization kinetics of semicrystalline polymers[7]. It turned out that the so-called long period that characterizes the

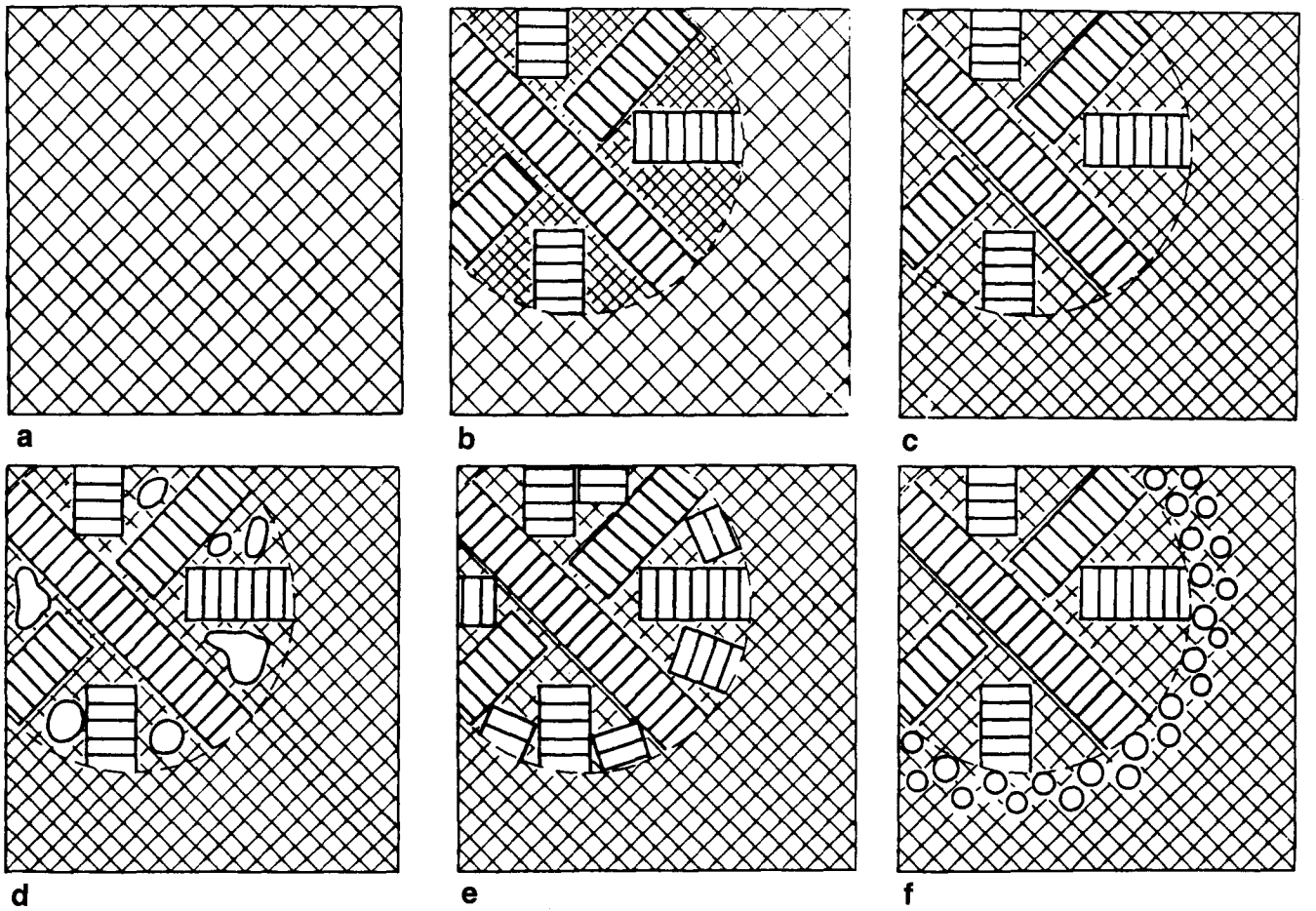

Figure 2 Schematic sketches of the phase separation phenomena that can accompany spherulitic crystallization. Grid density illustrates content of non-crystallizing component. Cf. also figure 4 in ref. 1. (a) Initial homogeneous melt. (b) Development of a spherulite containing crystalline lamellae. The composition of the spherulite amorphous areas is elevated, causing a concentration gradient at the spherulite surface. (c) Rapid diffusion caused concentration compensation on an intermediate composition level. (d) Phase separation within the amorphous parts of the spherulites at intermediate diffusion rates. Corresponds to (b) but with crossing the binodal composition. (e) Secondary crystallization of the intraspherulitic regions by creation of new lamellar stacks in the intralamellar regions by insertion crystallization. (f) Phase separation in the melt near the spherulite surface at intermediate diffusion rates. Corresponds nearly to (c) but surpassing the binodal composition

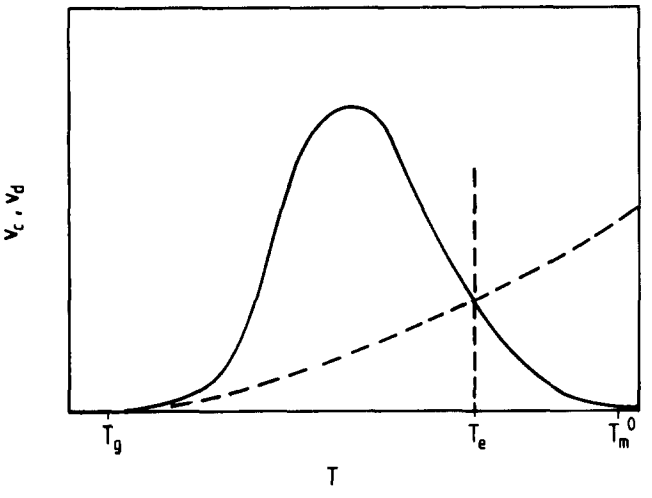

Figure 3 Rates of spherulite growth v_c (——) and diffusion v_d (– – –) vs. temperature T (schematically). T_g = glass transition temperature; T_m^0 = melt/crystal equilibrium temperature; T_e = crossover temperature

supermolecular arrangement of crystalline lamellae can change with time, i.e. with progressive crystallization, in several different ways. In some instances, an increase of the long period with crystallization time is observed, which can be caused by lamellar thickening[8]. A possible decrease of the long period with crystallization time, on the other hand, can originate from 'lamellar flattening'[7] or from 'insertion crystallization'[9]. In either case, then, the described temporal changes are linked with the post-crystallization step or secondary crystallization, i.e. with the changes of the crystalline structure within the spherulites, although the insertion crystallization scheme has been developed initially for the understanding of recrystallization phenomena. Distinction between the several schemes is possible by separate determination of lamellar and intralamellar thicknesses.

MATERIALS, PREPARATION, AND INVESTIGATION AND EVALUATION TECHNIQUES

The materials and the preparational routes were the same as those used previously[1] (*Table 1*). The samples (total thickness 1 mm) were melt homogenized for 10 min at a temperature 20°C above the melt/crystal coexistence temperature or the binodal temperature, respectively (cf. *Figure 1*). Isothermal crystallization at T_c was performed after quenching with (experimentally limited) rates ranging between -15°C min^{-1} ($T_c = 25$°C) and -30°C min^{-1} ($T_c = 45$°C). Simultaneously, the SAXS has been measured with synchrotron radiation (at HASYLAB/DESY, Hamburg, Germany) of 1.5 Å (sample–detector distance 2 m). The spatial resolution power of the used position-sensitive detector is 0.3 mm, i.e. $\Delta\theta = 10^{-2}$ deg or $\Delta s = 2\Delta\theta/\lambda = 2 \times 10^{-3}$ nm^{-1}. The intensity of the radiation source is about 1000-fold that of a copper X-ray tube at $\lambda = 1.54$ Å, this allowing reduction of registration time by the same factor. This, therefore, enables measurement of the temporal development of the scattering patterns. The patterns were recorded every 10 s. Subsequently, they were Fourier transformed, this yielding the structure autocorrelation function of the respective samples[10]. These functions, in turn, were evaluated with respect to lamellar and interlamellar thicknesses d_c and d_a, respectively, the sum of which yields the average lamellar distance ('long period'), specific internal surface S_i and crystal/amorphous interphase thickness d_i (ref. 11).

EXPERIMENTAL RESULTS

The temporal development of the scattering patterns is illustrated by *Figure 4*, where that of a blend with a PCL content of $c_{PCL} = 60$ wt% at $T_c = 35$°C is shown. Some of the structural parameters deduced therefrom are displayed in *Figures 5* to *8*. In *Figure 5*, the thickness d_c of the crystalline lamellae is displayed as a function of the crystallization time t_c for pure PCL at several crystallization temperatures T_c. It can be seen clearly that d_c is independent of time after a short crystallization induction time, and that d_c increases with increasing T_c. In contrast, the thickness d_a of the amorphous layers decreases gradually with time and increases with T_c, as can be seen from *Figure 6*, where this quantity is drawn for a blend with composition $c_{PCL} = 40$ wt%. The development of the thickness d_i of the crystalline–amorphous interface in the same sample is shown in *Figure 7*. It decreases with time at the same rate as d_a, and is the smaller the lower is T_c. Finally, from *Figure 8*, it can be seen that the amount S_i of this interface increases with time and decreases with increasing T_c in a blend with $c_{PCL} = 100$ wt%. The principal course of all these functions, however, is independent of composition.

In any case, the investigated structural parameters level off after a certain crystallization time. The dependences of $d_a^\infty = d_a(t \to \infty)$ and d_c^∞ on c_{PCL} and T_c are shown in *Figures 9* and *10*. Both these quantities increase with decreasing PCL content and increasing crystallization temperature. The S_i^∞ values are found to decrease slightly with increasing T_c and c_{PCL}. In contrast, the interface thicknesses d_i^∞ decrease strongly with increasing c_{PCL} but are, within the limits of the experimental error, independent of the crystallization temperature (*Figure 11*).

The crystallization half-times τ_c as found from the functions $d_a(t)$, $d_i(t)$ and $S_i(t)$ are shown in *Figure 12*. They are nearly constant (τ_c^0) at lower crystallization temperature but increase drastically above a critical T_c value (T_c^0). These dependences coincide quantitatively with those found by d.s.c. measurements[12], by the temporal development of the SAXS scattering intensity[6] and, for the pure PCL, by other authors[13].

Basically, any $\tau_c(T_c)$ curve can be divided into a 'low'-temperature branch (L), which is determined by the vicinity of T_g (τ_c is the larger the nearer T_g is), and a 'high'-temperature branch (H), the course of which is determined essentially by the equilibrium melting temperature. Inspection of *Figure 12* reveals that, for our samples, 'low' and 'high' crystallization temperatures

Table 1 Sample materials

	PCL	Atactic PS
Grade/supplier	PCL 300/Union Carbide	Polymer Standard Service
T_g (°C)	−69	19
T_m^0 (°C)	69	–
ΔH^0 (J g^{-1})	135	–
M_n (g mol^{-1})	10000	770
M_w (g mol^{-1})	15000	840

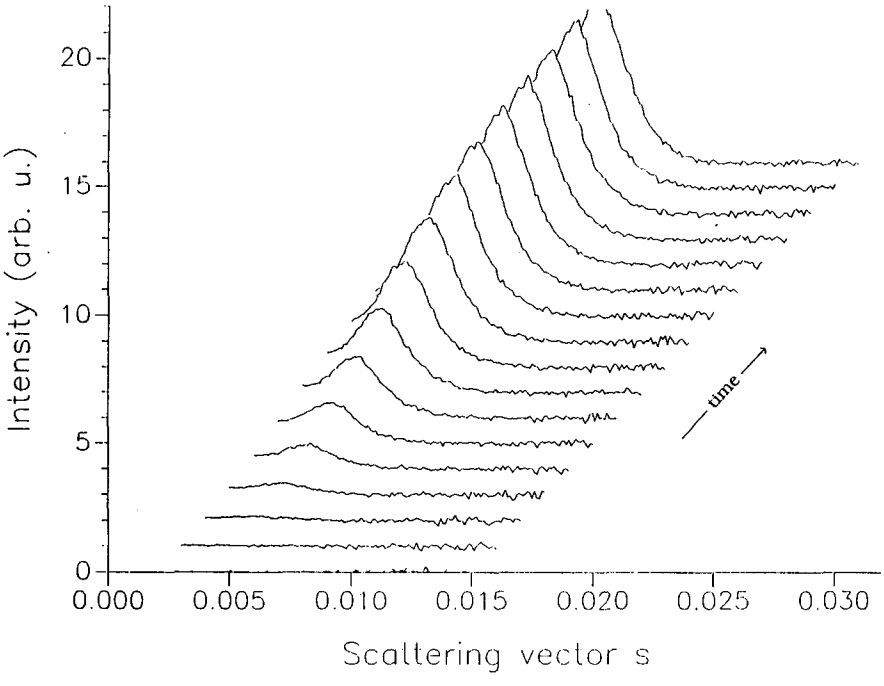

Figure 4 Temporal development of the scattering patterns (scattering vector $s = 2(\sin\theta)/\lambda$) of a blend $c_{PCL} = 60$ wt% at $T_c = 35°C$

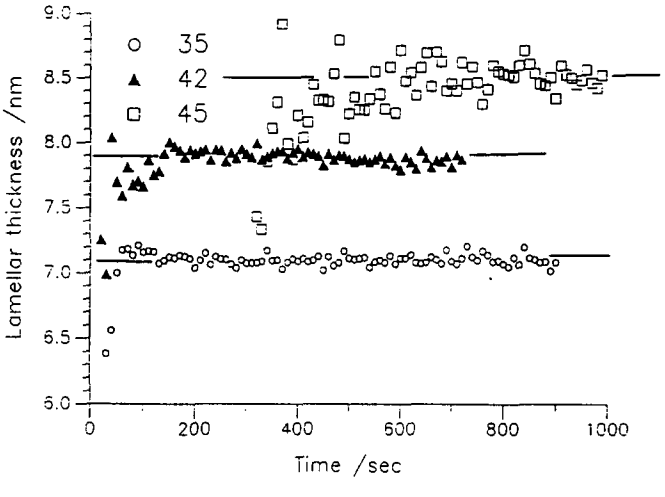

Figure 5 Thickness d_c of the crystalline lamellae as a function of the crystallization time t_c for pure PCL. Parameter: crystallization temperature, T_c (°C)

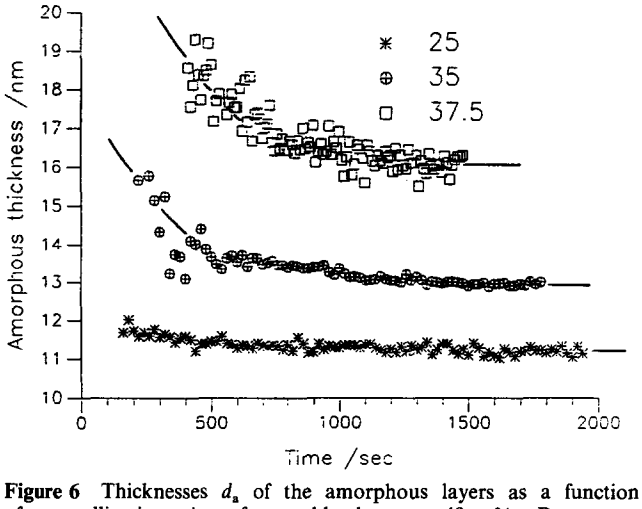

Figure 6 Thicknesses d_a of the amorphous layers as a function of crystallization time for a blend $c_{PCL} = 40$ wt%. Parameter: crystallization temperature, T_c (°C)

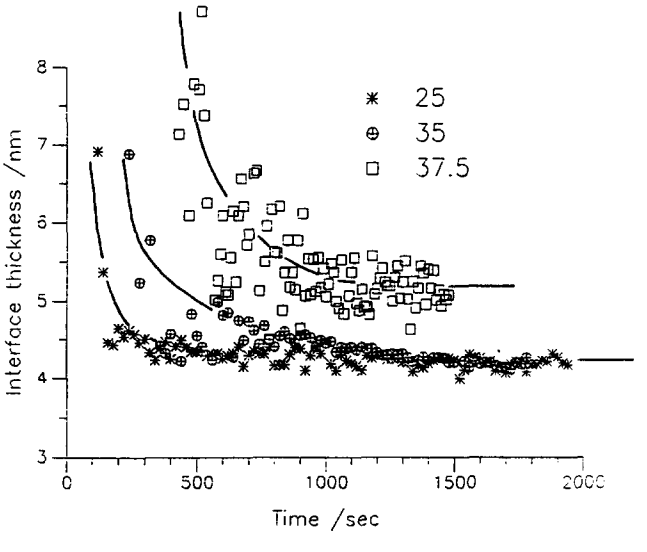

Figure 7 Development of the thickness d_i of the crystalline–amorphous interface with crystallization time t_c for a blend $c_{PCL} = 40$ wt%. Parameter: crystallization temperature, T_c (°C)

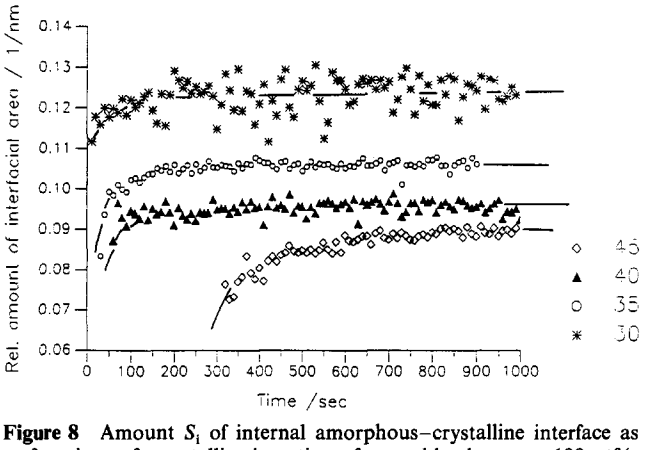

Figure 8 Amount S_i of internal amorphous–crystalline interface as a function of crystallization time for a blend $c_{PCL} = 100$ wt%. Parameter: crystallization temperature, T_c (°C)

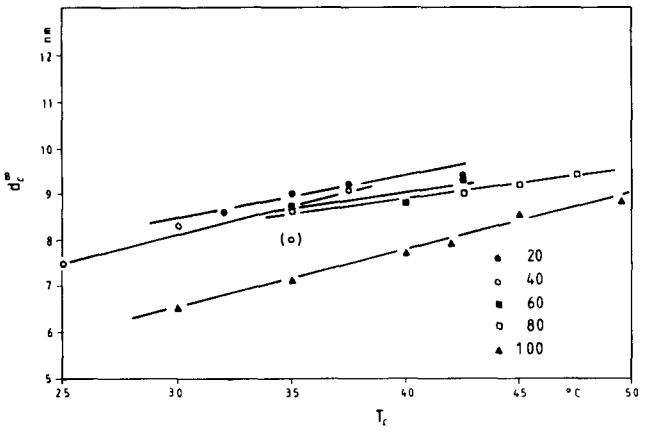

Figure 9 Dependence of $d_c^\infty = d_c(t \to \infty)$ on crystallization temperature T_c. Parameter: composition, c_{PCL} (wt%)

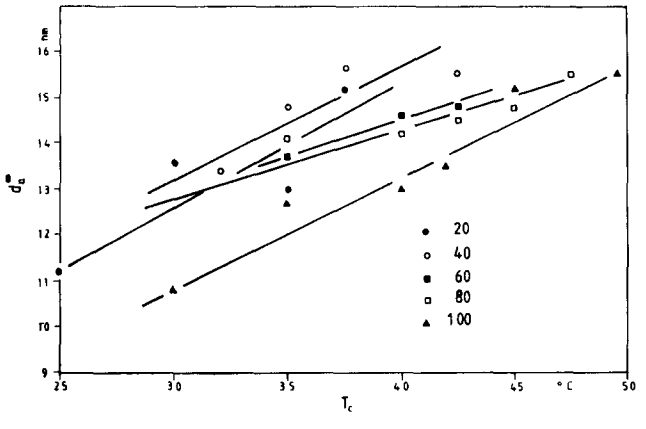

Figure 10 Dependence of $d_a^\infty = d_a(t \to \infty)$ on crystallization temperature T_c. Parameter: composition, c_{PCL} (wt%)

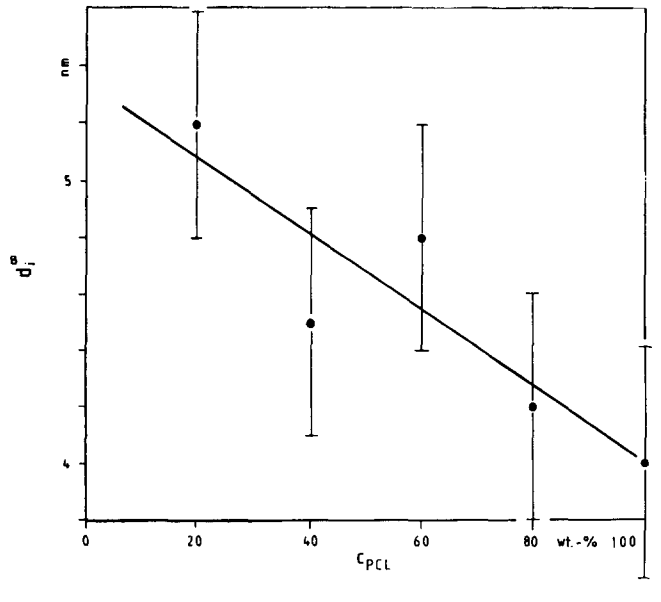

Figure 11 Interface thickness d_i^∞ as a function of the composition c_{PCL}

are separated at 30–35°C. Considering the particular course of the respective curves here, we describe the position and the course of these two branches by suitable but basically different parameters: L is characterized by the crystallization half-time at a suitable reference 'low' crystallization temperature (τ_c^0) since τ_c is almost not changing in that temperature range, and H is characterized by the temperature at which τ_c suddenly increases (T_c^0). The dependences of $\tau_c^0 = \tau_c(25°C)$ and T_c^0 on composition are given in *Figure 13*.

DISCUSSION

It should be recalled that all the figures reflect, essentially, the development of the crystalline structure, particularly the lamellar stacking, within the spherulites. The overall effect, however, is a superposition of the contributions of spherulites that are created at different times according to a separate temporal law. We found a coincidence of the time functions of d.s.c.[12] and SAXS measurements and the growth rate of spherulites as detected by light microscopy[1,6] or light transmittance[6] as well. This reveals that the creation and growth of spherulites as well as the changes of their internal structure ('post-crystallization' or 'secondary crystallization') proceed on the same timescale. This makes the discussion of the absolute values of the half-times as presented in *Figures 12* and *13* ambiguous. The principal course of temporal developments, nevertheless, should be discussed in terms of the structural changes within the spherulites alone. From the rough equality of the mentioned time functions, on the other hand, separate conclusions can be

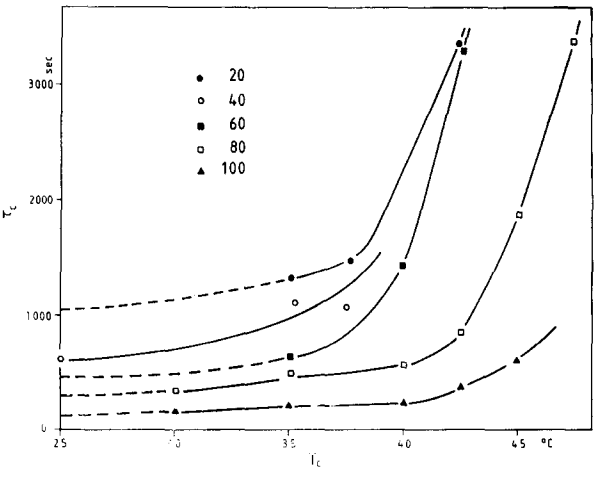

Figure 12 Crystallization half-times τ_c as a function of crystallization temperature T_c. Parameter: composition, c_{PCL} (wt%)

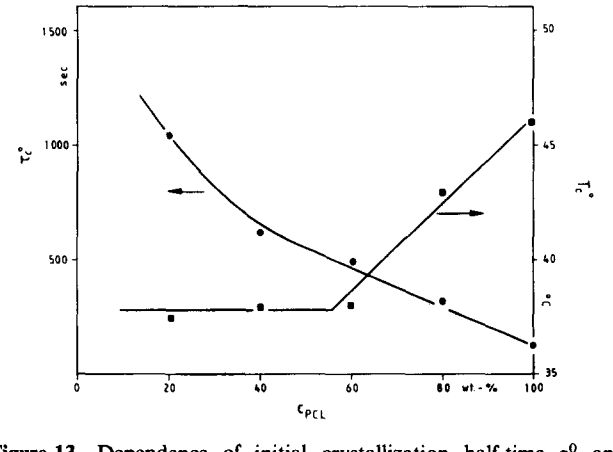

Figure 13 Dependence of initial crystallization half-time τ_c^0 and critical crystallization temperature T_c^0 on composition c_{PCL}

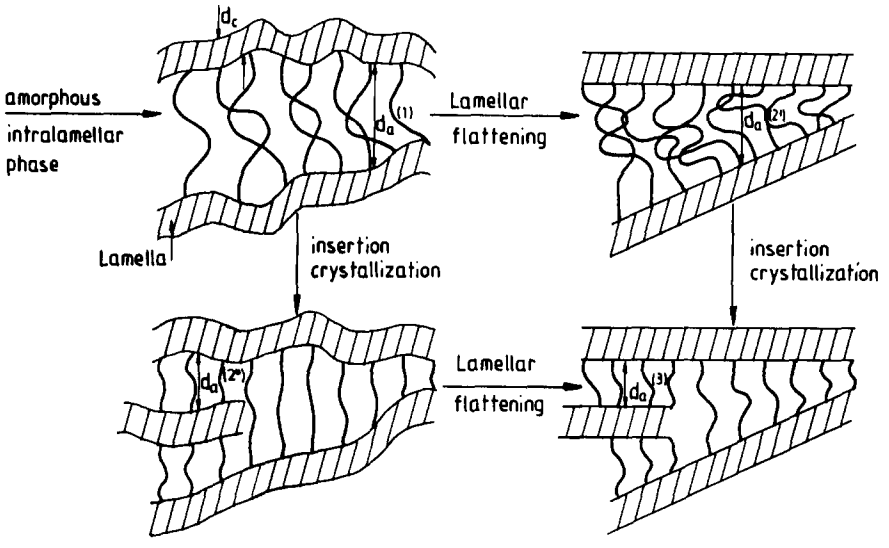

Figure 14 Change of supermolecular structure during post-crystallization. (a) Initial stage: existence of wavy, bent lamellae with a rather broad amorphous gap. (b) Lamellar flattening: temperature-dependent healing of defects in the lamellae makes their surface even and lets the amorphous gap relax and narrow. (c) Insertion crystallization: again depending on the temperature, the amorphous gap can crystallize, thus additionally decreasing the thickness of the amorphous gap and increasing the amount of crystalline/amorphous interface. Processes (b) and (c) can proceed nearly simultaneously

drawn on the structure development processes, as will be outlined at the end of this section.

The first thing that can be derived from the figures is that the X-ray degree of crystallinity $x_{cs}^{\infty} = d_c^{\infty}/(d_c^{\infty} + d_a^{\infty})$ within the spherulitic lamellar stacks (which, in the sense of the preceding remark, can differ from the overall degree of crystallinity x_c) is independent of composition and crystallization temperature and amounts to about 40%. Considering the binodal compositions at several T_c values and the temporal development of x_{cs}, it turns out that the amorphous phase between the lamellae must at least reach the binodal composition if $c_{PCL} < 70$ wt%. Its composition may even be in the miscibility gap if the PS that is released by the PCL crystallization cannot diffuse into the melt or, at least, away from the lamellar bundles. This should apply particularly at lower crystallization temperature, where the spherulite growth rate significantly exceeds that of diffusion (cf. *Figure 3*). On the other hand, basically, the crystallization gradually slows down when approaching the glass transition temperature T_g. At a given 'low' crystallization temperature, consequently, the crystallization rate is indicative of the distance to T_g. The continuous decrease of the secondary crystallization rate with decreasing PCL content of the blend at low T_c values as expressed by the function $\tau_c^0(c_{PCL})$ (*Figure 13*) suggests therefore a likewise continuous increase of glass transition temperature of the spherulite amorphous phase with c_{PCL}. Reconsidering *Figure 1*, it must therefore be concluded that at lower crystallization temperature the amorphous phase between the lamellae does not decompose when reaching the binodal composition – at least not completely – but, instead, stays homogeneously mixed with a supersaturated composition c^s. The strength of this supersaturation $(c_{binodal} - c^s)$ increases gradually with increasing content of PS in the starting material. This conclusion is supported by *Figure 11*, which indicates that the crystal–amorphous interface thickness also increases continuously with increasing PS content of the starting material. The experiment, however, yields no information on the strength of supersaturation as defined above. Obviously, the limited diffusion rate not only prevents the migration of the surplus PS away from the lamellar stacks into the melt and, consequently, causes its capture in the growing spherulite. Moreover, it also inhibits coagulation and phase separation of the released PS in the interlamellar amorphous phase. The diffusion-limited insertion into spherulites has been observed and detected by SAXS already in the system PCL/(styrene–maleic anhydride copolymer), which, however, is compatible in the whole composition range[14].

In contrast, at higher crystallization temperatures, the PS that is released by PCL crystallization should be able to diffuse completely or, at least, to some extent into the surrounding melt. This, in turn, would allow approach to the thermodynamic equilibrium composition in the amorphous phase of the spherulites, i.e. the binodal composition for the samples with $c_{PCL} < 70$ wt%. The crystallization kinetics at higher T_c values, consequently, should then become nearly independent of the composition for this c_{PCL} range. This has indeed been observed (*Figure 12*, where the graphs for the respective compositions nearly coincide) and is also illustrated by the function $T_c^0(c_{PCL})$ (*Figure 13*), which levels off for that composition range.

Clearly, there is a gradual transition from the one regime to the other when changing the crystallization temperature. There must exist, therefore, an intermediate crystallization temperature range where diffusion is possible to a limited extent that certainly allows removal of released PS from the developing lamellar stacks but not its migration down to the surrounding melt. In contrast, a separate melt-like amorphous phase may develop inside the spherulites between the lamellar bundles. It is a matter of opinion if this phase is considered to be separated from the crystallizing volume or if it is a melt area that is engulfed by the growing spherulite. In either case, the composition of this phase

should be intermediate to that of the melt and the amorphous regions between the lamellae. Such a phase would cause a distinctly irregular internal structure of the spherulites, which has indeed been observed by light microscopy for the corresponding mixtures and treatment temperatures[1,6]. This phase, if present, as well as occasional phase separation phenomena within it should be detectable by electron microscopy. Corresponding investigations are in progress. This phase, principally, is moreover able to crystallize. It could, consequently, play an important part during the post-crystallization step by the creation of new lamellar stacks within the spherulites and by insertion crystallization, as will be outlined in more detail below. These crystallization processes, in turn, would then proceed at a rate comparable to that of overall spherulite growth, as indeed has been observed.

The decrease of d_a with time (*Figure 6*) as well as the temporal constancy of d_c (*Figure 5*) can be explained by a gradual improvement of the lamellar habit (*Figure 14*). The initially disturbed structure consists of wavy lamellae with bent surfaces. This, in turn, keeps adjacent lamellae strictly separated. A temporal improvement of this structure lets the lamellae flatten without changing their thicknesses but with the possibility to bring them closer[7]. Moreover, the simultaneous increase in the amount of crystal/amorphous interface (*Figure 8*) indicates that, additionally, the broad and relaxed amorphous phase between the lamellae or elsewhere within the spherulites post-crystallizes according to a scheme comparable to insertion crystallization[9]. The decrease of S_i^∞ with increasing PS content may hint that the PS disturbs insertion crystallization, possibly because of the rise in glass transition temperature.

REFERENCES

1 Li, Y., Stein, M. and Jungnickel, B.-J. *Colloid Polym. Sci.* 1991, **269**, 772
2 Tanaka, H. and Nishi, T. *Phys. Rev. Lett.* 1985, **55**, 1102
3 Tanaka, H. and Nishi, T. *Phys. Rev.* (*A*) 1989, **39**, 783
4 Shibanov, Y. D. and Godovski, Y. K. *Prog. Colloid Polym. Sci.* 1989, **80**, 110
5 Shibanov, Y. D. and Godovski, Y. K. *Colloid Polym. Sci.* 1985, **263**, 202
6 Li, Y., PhD Thesis, Technische Hochschule Darmstadt, 1991
7 Elsner, G., Riekel, C. and Zachmann, H. G. *Adv. Polym. Sci.* 1985, **67**, 1
8 Barham, P. J. and Keller, A. *J. Polym. Sci., Polym. Phys. Edn.* 1989, **27**, 1029
9 Strobl, G. R., Engelke, T., Meier, H. and Urban, G. *Colloid Polym. Sci.* 1982, **260**, 394
10 Kratky, O. and Glatter, O. 'Small Angle X-Ray Scattering', Academic Press, London, 1982
11 Strobl, G. R. and Schneider, M. J. *J. Polym. Sci., Polym. Phys. Edn.* 1980, **18**, 1343
12 Stein, M., Master's Thesis, Technische Hochschule Darmstadt, 1990
13 Nojima, S., Tsutsui, H., Urushihara, M., Kosaka, W., Kato, N. and Ashida, T. *Polym. J.* 1986, **18**, 451
14 Defieuw, G., Groeninckx, G. and Reynaers, H. *Polymer* 1989, **30**, 2158
15 Fox, T. G. *Bull. Am. Phys. Soc.* 1956, **1**, 123